Pulse Radiolysis of Supercritical Water. 2. Reaction of Nitrobenzene with Hydrated Electrons and Hydroxyl Radicals†

ARTICLE *in* THE JOURNAL OF PHYSICAL CHEMISTRY A · DECEMBER 2002

Impact Factor: 2.69 · DOI: 10.1021/jp026812u

5 AUTHORS, INCLUDING:

Timothy W Marin
Benedictine University
54 PUBLICATIONS **805** CITATIONS
SEE PROFILE

Jason A. Cline
Spectral Sciences Incorporated
35 PUBLICATIONS **399** CITATIONS
SEE PROFILE

Kenji Takahashi
Kanazawa University
97 PUBLICATIONS **1,251** CITATIONS
SEE PROFILE

Pulse Radiolysis of Supercritical Water. 2. Reaction of Nitrobenzene with Hydrated Electrons and Hydroxyl Radicals†

Timothy W. Marin, Jason A. Cline, Kenji Takahashi,‡ David M. Bartels,* and Charles D. Jonah

Chemistry Division, Argonne National Laboratory, Argonne, Illinois 60439

Received: August 21, 2002; In Final Form: October 1, 2002

The rate constants for the reactions of nitrobenzene with the hydroxyl radical ($OH^•$) and hydrated electron ($(e^-)_{aq}$) in water have been measured from room temperature to 400 °C using electron pulse radiolysis and transient absorption spectroscopy. The diffusion-limited reaction of nitrobenzene with $(e^-)_{aq}$ exhibits temperature-insensitive activation energy up to 300 °C, indicating that the activation energy for electron diffusion remains high over this range. The $(e^-)_{aq}$ reactivity is explained as a long-range electron transfer, and the results are interpreted in terms of extended Marcus theory and Smoluchowski relationships. At 380 °C, the rate constant has a density dependence similar to that previously reported for other $(e^-)_{aq}$ scavenging reactions. The reaction rate of nitrobenzene with $OH^•$ is very insensitive to temperature from room temperature up to 300 °C, in agreement with previous studies. Above 300 °C, the rate constant increases as the critical temperature is approached and exceeded. Time-resolved electronic absorption spectra of the nitrobenzene radiolysis transients reveal complex kinetics involving multiple absorbing species.

I. Introduction

Recent designs for more economic and thermally efficient water-cooled nuclear reactors would operate the primary cooling loop at higher temperatures and pressures that exceed the critical point of water (374 °C, 221 bar).[1−3] The radiation-induced chemistry of water remains largely unknown under these conditions, and most of its reactions have been measured only up to 250 °C (or less).[4] Water radiolysis has crucial implications for the corrosion processes occurring in the primary cooling loop of the reactor.[3,5,6] This manuscript is the second in a series that addresses the radiation-induced chemistry of water at supercritical temperatures and pressures and provides representative data for the reactivities of radiolytically produced species.[7]

Hydrated electrons ($(e^-)_{aq}$) and hydroxyl radicals ($OH^•$) represent two of the primary species formed in water radiolysis. It is therefore necessary to understand their individual reactivities and roles in water radiation chemistry. To date, few experiments have been carried out to discern their reactivities in supercritical water. We perform pulse radiolysis followed by transient absorption to follow the kinetics of $(e^-)_{aq}$ and $OH^•$ scavenging by nitrobenzene. Nitrobenzene has been shown to be reactive toward both species.[8−27] Experimentally monitoring the reactions of $(e^-)_{aq}$ and $OH^•$ with nitrobenzene is easy because both reactions are characterized by strong visible absorption changes (discussed below). This makes nitrobenzene a convenient reference partner for competition kinetic studies of other $OH^•$ scavengers.

The reaction of nitrobenzene with $(e^-)_{aq}$ forms a nitrobenzene radical anion

$$C_6H_5NO_2 + (e^-)_{aq} \rightarrow C_6H_5NO_2^{•-} \qquad (1)$$

The process has been shown to be diffusion-controlled at temperatures up to 200 °C.[25] A motivation for the current work was to determine whether reaction 1 exhibits diffusion-controlled behavior up to supercritical conditions, which could give insight into the electron diffusion coefficient over this temperature range. The present study extends previous measurements up to 400 °C and reports the density dependence of the reaction rate at 380 °C, just above the critical temperature.

The addition of $OH^•$ to nitrobenzene forms the nitrohydroxycyclohexadienyl radical

$$C_6H_5NO_2 + OH^• \rightarrow C_6H_5NO_2(OH^•) \qquad (2)$$

A recent pulse radiolysis study examined this reaction up to 390 °C and showed that the rate constant is very insensitive to temperature up to 350 °C.[12] Above the critical point, the rate constant was shown to increase approximately two-fold. The $C_6H_5NO_2(OH^•)$ product has a strong visible absorption in the 400 nm region, making reaction 2 a useful reference to gauge against $OH^•$ reactivity with other species. We have repeated previous measurements[11,12] to confirm reported rate constants in preparation for a study of the $OH^• + H_2$ reaction. Time-resolved spectra of the nitrobenzene radiolysis transients reveal complex kinetics involving multiple absorbing species. Most notably, it appears that $H^•$ atom addition to nitrobenzene strongly interferes with the measurement of $OH^•$ kinetics at temperatures above 300 °C.

II. Experimental Section

Pulse radiolysis/transient absorption experiments were carried out using 4 ns pulses from the Argonne Chemistry Division's

† Work performed under the auspices of the Office of Science, Division of Chemical Science, US-DOE under Contract No. W-31-109-ENG-38. Additional funding was provided under Nuclear Energy Research Initiative grant No. M9SF99-0276 and the Ministry of Education in Japan.

* To whom correspondence should be addressed.

‡ Present address: Division of Quantum Energy Engineering, Hokkaido University, Sapporo 606-8628, Japan.

10.1021/jp026812u CCC: $22.00
Published on Web 12/03/2002

20 MeV electron linac accelerator. The sample cell and flow system were described in our previous publications.[7,28] A Faraday block on a shutter placed before the sample cell was used to check the charge per pulse (dose) periodically to ensure similar pulse amplitudes over the course of a day. Typical dose fluctuations over a day were ±5% and shot-to-shot variations were ±2%.

Analyzing light was obtained from a 75 Watt xenon arc lamp, pulsed for ~300 μs. The lamp pulse was timed so that the linac pulse coincided with the most stable, flattest portion of the lamp response. For $(e^-)_{aq}$ scavenging experiments, the decay of the $(e^-)_{aq}$ absorption spectrum was monitored. Because the $(e^-)_{aq}$ absorption spectrum is sensitive to both temperature and density, wavelengths for electron scavenging experiments were chosen to coincide with the absorption maximum at each temperature. (The red shift and width of the $(e^-)_{aq}$ spectrum at elevated temperatures will be the subject of a future publication.[29]) Wavelengths were selected using 10 nm bandwidth interference filters (Andover Corporation) and ranged from 750 to 1200 nm. A germanium photodiode (Germanium Power Devices GMP566) was used for detection. The small correction needed for its non-single-exponential response has been described in detail.[30] The wavelength for $OH^\bullet$ scavenging experiments was 400 nm and was isolated using a 40 nm bandwidth interference filter. Time-resolved spectra of the nitrohydroxycyclohexadienyl radical were acquired from 400 to 520 nm using 10 nm bandwidth interference filters and a silicon photodiode (EG&G FFD-100) and from 320 to 390 nm using a monochromator (Photon Technologies SID-101) and photomultiplier (Hamamatsu R1913).

The flow system and sample cell have been described previously.[7,28] Details pertaining to these experiments and slight modifications to the flow system are given below. Two sample reservoirs were used simultaneously in $(e^-)_{aq}$ scavenging experiments, one containing deionized water (18.2 MΩ-cm, Barnstead Nanopure system) and the other a solution of nitrobenzene (Sigma-Aldrich, 99+%) in water. The nitrobenzene concentration was verified via UV/Vis absorption ($\epsilon_{268.5nm}$ = 7800 $M^{-1}cm^{-1}$). Both water reservoirs contained 10^{-5} M KOH (diluted from Sigma-Aldrich 0.991 N standard) to eliminate $(e^-)_{aq}$ scavenging by protons and were continuously purged with ambient pressures of Ar. For $OH^\bullet$ scavenging reactions, KOH was not added, and both reservoirs were initially saturated with N_2O or O_2 for ~30 min and kept sealed with a slightly pressurized headspace over the course of experiments, giving N_2O and O_2 concentrations of 0.024 and 0.0013 M, respectively. N_2O and O_2 serve as electron and electron/$H^\bullet$ atom scavengers, respectively. N_2O was used for all measurements up to 275 °C, and O_2 was used for all measurements at 300 °C and above. Use of N_2O in these experiments has the added advantage of rapidly generating additional $OH^\bullet$ via

$$N_2O + (e^-)_{aq} \rightarrow O^{\bullet-} + N_2 \quad (3)$$

$$O^{\bullet-} + H_2O \rightarrow OH^- + OH^\bullet \quad (4)$$

and thus is preferred for use below 300 °C. As discussed below, the switch is made to O_2 at 300 °C and above to aid in scavenging the greater yield of $H^\bullet$ atoms in this temperature range.[7]

In all experiments, the concentration of nitrobenzene was controlled by changing the scavenger solution flow rate relative to the pure water flow rate using two independent HPLC pumps (Alltech 301). System pressure was maintained by restricting the system output flow with a length of stainless steel capillary tubing. The capillary tubing was immersed in a controllable temperature bath. The bath temperature was adjusted to change the water viscosity. With a fixed flow rate controlled by the HPLC pumps, this viscosity adjustment regulates the sample pressure. System pressure and temperature were continuously monitored during the experiments via a piezoelectric pressure transducer (Omega PX02 series) and thermocouples. Normal system stabilities were ±0.2 °C and ±0.1 bar. System flow rates were generally 2.0−2.5 mL/min, adjusted as necessary to set the proper pressure. Each time the nitrobenzene concentration was changed, the system was flushed for 3−4 min to ensure adequate time for sample renewal in the flow system and sample cell.

Previous supercritical water oxidation experiments have shown that nitrobenzene decomposed in supercritical water at 440 °C;[31,32] however, its stability was confirmed under the present concentration and temperature conditions. Spectra of nitrobenzene samples were taken after passing through the sample cell with both N_2O and O_2 present at various temperatures and were compared to spectra taken before heating. No degradation of the nitrobenzene was observed up to 400 °C, even in the presence of O_2.

III. Results and Discussion

A. Hydrated Electron Scavenging. In this section, we first present the experimental kinetic results and data analysis of the $(e^-)_{aq}$ reactivity with nitrobenzene. We then explain the $(e^-)_{aq}$ reactivity in terms of long-range electron transfer. The results are interpreted in terms of extended Marcus theory and Smoluchowski relationships.

1. Kinetics. A survey of hydrated electron scavenging by nitrobenzene (reaction 1) was carried out as a function of temperature up to 400 °C by monitoring the decay of the intense hydrated electron absorption in the near-infrared. All data were collected at a pressure of 240−250 bar except at 400 °C, where the pressure was 300 bar, and at 380 °C, where data were taken at a series of pressures. In the limit of high nitrobenzene concentration, the production of nitrobenzene anion occurs via pseudo-first-order kinetics and the observed rate depends linearly on the nitrobenzene concentration. The applied dose was adjusted to give $(e^-)_{aq}$ concentrations of ~5×10^{-7} M, and all nitrobenzene concentrations used were greater than 4×10^{-6} M to ensure pseudo-first-order kinetics. Five nitrobenzene concentrations were run at each temperature/pressure state point, as well as a zero concentration. The fitted rates were plotted versus initial concentration (concentration at room temperature before heating and pressurizing) and showed a linear concentration dependence. The slope divided by the density of water at each temperature was taken as the reaction rate constant.

Typical fitted kinetic data taken at 300 °C are shown in Figure 1, and the corresponding pseudo-first-order plot showing the concentration dependence of the fitted rate is shown in the inset. The decays shown are the $(e^-)_{aq}$ transient absorption at 900 nm. Nitrobenzene concentrations range from 4.4×10^{-6} to 2.2×10^{-5} M, corresponding to the longest through shortest observed decay rates (0 concentration trace not shown on plot). The curves were fitted starting approximately 35 ns after the linac pulse to avoid minor distortions from linac noise and spur recombination chemistry.

An Arrhenius plot for reaction 1 is shown in Figure 2, and fitted rate constants are given in Table 1. Vertical error bars reflect statistical errors arising from the fits shown in Figure 1, and most are on the order of the data point size. We have extrapolated an Arrhenius fit of data taken up to 100 °C by

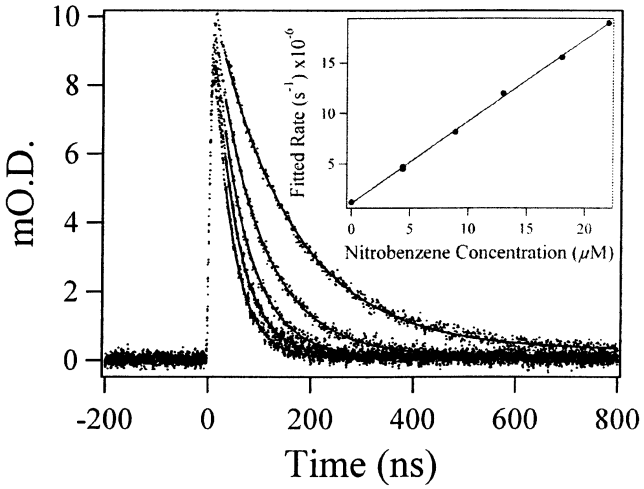

Figure 1. Sample fitted data for hydrated electron scavenging by nitrobenzene at 300 °C and 250 bar. Nitrobenzene concentrations range from 4.4×10^{-6} to 2.2×10^{-5} M, corresponding to the longest through shortest observed decay rates (0 concentration trace not shown in raw data). Inset: pseudo-first-order plot illustrating the concentration dependence of the observed hydrated electron scavenging rate at 300 °C.

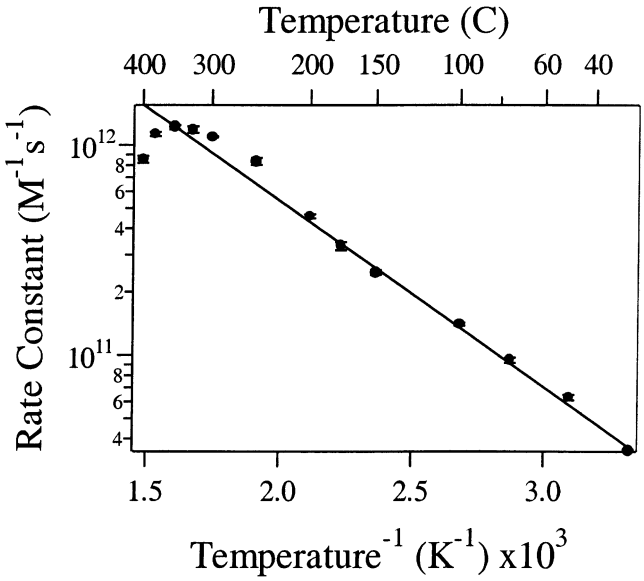

Figure 2. Arrhenius plot for the reaction of nitrobenzene with hydrated electrons. An Arrhenius fit to previous data[22] taken up to 100 °C is extrapolated to higher temperatures and superimposed for comparison.

TABLE 1: Fitted Rate Constants for Hydrated Electron Scavenging by Nitrobenzene (Reaction 1)

temp (C)	rate constant $(M^{-1}s^{-1}) \times 10^{-10}$	temp (C)	rate constant $(M^{-1}s^{-1}) \times 10^{-10}$
28	3.53 ± 0.04	250	83.4 ± 3.2
50	6.27 ± 0.19	300	109 ± 1
75	9.43 ± 0.28	325	118 ± 4
100	14.0 ± 0.2	350	122 ± 3
150	24.7 ± 0.7	380	113 ± 3
175	33.0 ± 1.4	400	85.3 ± 3.2
200	45.7 ± 1.0		

Freeman and co-workers[22] and superimposed it for comparison. Clearly, our measurements agree quite well with the previously reported activation energy up to ~200 °C. From 175 °C up to the critical region, the new data exceed the extrapolated Arrhenius values. Above the critical temperature, the rate constants cross over and then undershoot the extrapolation.

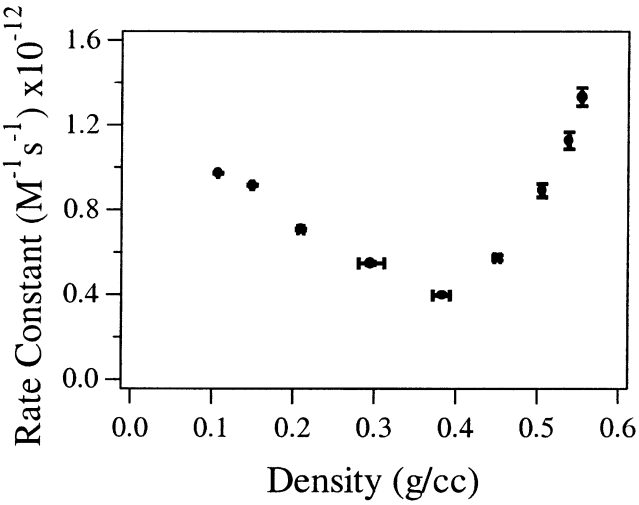

Figure 3. Effect of density on the rate constant for hydrated electron scavenging by nitrobenzene at 380 °C, just above the critical temperature of 374 °C.

TABLE 2: Fitted Rate Constants for Density Dependence of Hydrated Electron Scavenging by Nitrobenzene at 380 °C

pressure (bar)	density (g/cm^3)	rate constant $(M^{-1}s^{-1}) \times 10^{-11}$
190	0.107	9.72 ± 0.02
215	0.150	9.16 ± 0.04
230	0.209	7.07 ± 0.04
235	0.295	5.48 ± 0.07
240	0.383	3.97 ± 0.02
250	0.451	5.74 ± 0.12
275	0.506	8.92 ± 0.33
305	0.538	11.27 ± 0.40
325	0.554	13.33 ± 0.43

The density dependence of the rate constant at 380 °C is illustrated in Figure 3. Fitted rate constants are reported in Table 2. Data were obtained at nine different pressures ranging from 190 to 325 bar, corresponding to a density range of 0.11−0.55 g/cm^3. Because this represents a region where water is highly compressible, the density is very sensitive to minor pressure and temperature changes. Horizontal error bars are given to indicate possible density fluctuations. A sharp drop in the rate constant is seen as we proceed from the highest density down to ~0.40 g/cm^3. Continuing to yet lower densities, the rate constant increases again. A very similar trend has been observed previously for reactions between $(e^-)_{aq}$ and other hydrophobic species in supercritical water. The behavior was ascribed to the potential of mean force separating the $(e^-)_{aq}$ from the hydrophobic species in a compressible fluid.[7] We do not ascribe the behavior to $(e^-)_{aq}$ diffusion because the reaction of H$^\bullet$ atoms with OH^- has the same density dependence well below the diffusion limit.[7]

2. Electron-Transfer Model. Previous reports have demonstrated that there are few reactions that are truly diffusion controlled in water over a wide temperature range.[4,25,33] Many reactions that appear to be diffusion-limited near room-temperature become limited by some small activation barrier as the temperature is increased. Reaction 1 was claimed to demonstrate "diffusion-limited" behavior up to 200 °C,[25] but this claim was made without knowledge of the $(e^-)_{aq}$ diffusion rate. The activation energy for $(e^-)_{aq}$ diffusion in water measured up to 100 °C is 20.3 kJ/mol.[33] The same activation energy applies to the diffusion-limited bimolecular recombination of two electrons up to 150 °C.[34] Consequently, it can be assumed that the diffusion-limited activation energy for a reaction involving $(e^-)_{aq}$

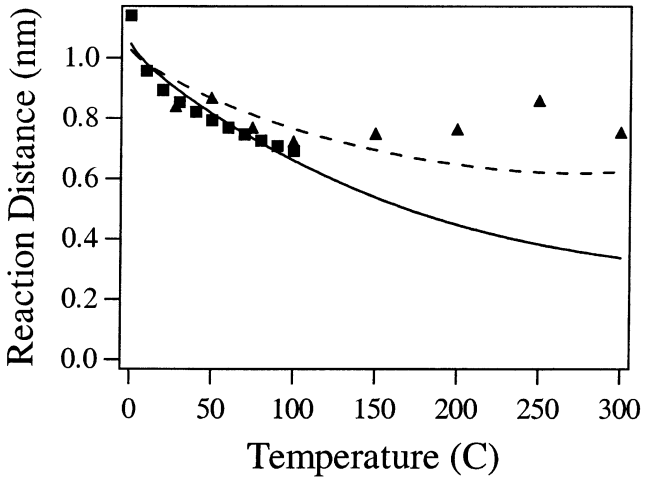

Figure 4. Temperature dependence of the average reaction distance for hydrated electron scavenging by nitrobenzene, calculated using the Smoluchowski equation with measured reaction rates. Data by Freeman et al.[22] below 100 °C (squares) and the current data (triangles) up to 300 °C are shown, along with fits obtained with eq 9. The solid curve is the fit to data obtained by Freeman and the dashed line is the best fit to both data sets, assuming temperature independence of α and β.

should be 20.3 kJ/mol up to 150 °C and also at higher temperatures if the $(e^-)_{aq}$ diffusional activation energy remains constant. Analysis of the data points in Figure 2 from room temperature up to 100 °C gives a value of 17.6 ± 0.8 kJ/mol, similar to previous reports.[18−24,26,27] The slope remains nominally the same within error limits up to 150 °C. It was argued by Schmidt et al.[33] that reaction 1 is a diffusion-limited, long-range electron transfer process, which accounts for its activation energy slightly below 20.3 kJ/mol in the low-temperature region (see below). There is an apparent increase in the activation energy of reaction 1 from 150 °C up to where the rate begins turning over near 300 °C, and fitting the slope from 150 to 300 °C gives a value of 20.8 ± 1.1 kJ/mol. These values suggest essentially diffusion-limited behavior for reaction 1 from room temperature up to 300 °C. Above 300 °C, we have insufficient information to make this assertion.

Assuming a diffusion-limited reaction, from the experimental data, we can calculate the average reaction distance R at each temperature using the Smoluchowski equation[35,36]

$$k = 4\pi RD \tag{5}$$

where k is the diffusion-limited rate constant at each temperature and $D = D_a + D_b$ is the relative diffusion coefficient of reactants a and b. Diffusion coefficients for $(e^-)_{aq}$ are extrapolated from data below 100 °C.[33] On the basis of previous measurements,[37] nitrobenzene diffusion coefficients are assumed to follow Stokes−Einstein behavior in water, scaling as $T/\eta(T)$, where $\eta(T)$ is the temperature-dependent viscosity of water. Figure 4 illustrates the calculated reaction distance for both the current data and data obtained by Freeman et al.[22] Note that the shortest reaction distance estimated is ∼0.7 nm at 100 °C. The nitrobenzene radius may be estimated as a constant 3.6 Å from the van der Waals' equation of state for benzene.[38] A temperature-dependent $(e^-)_{aq}$ radius in the 2.4−4.0 Å range can be estimated from moment analysis modeling of the $(e^-)_{aq}$ absorption spectra,[29] where the radius becomes larger with increasing temperature. The large average reaction distances strongly suggest that reaction 1 occurs as a long-range reaction of a solvent-separated pair even up to 300 °C rather than a traditional diffusion-limited reaction that occurs upon "contact" of the reactants.

The long-range electron-transfer reaction of $(e^-)_{aq}$ with nitrobenzene can be viewed in terms of the $(e^-)_{aq}$ moving from its solvent potential well into a potential well centered on the nitrobenzene. Such a process can be analyzed in terms of extended Marcus theory. The result of Marcus theory and its extensions incorporating quantum vibrational degrees of freedom is an electron-transfer rate expression taking the form[39−43]

$$W(R,T) = \frac{H_{ab}{}^2}{\hbar}\left(\frac{\pi}{\lambda k_B T}\right)^{1/2} \sum_{n_f} e^{-S}\frac{S^{n_f}}{n_f!} \exp\left[-\frac{(\Delta G + \lambda + n_f h\nu)^2}{4\lambda k_B T}\right] \tag{6}$$

where λ is the solvent reorganization energy, H_{ab} is the electronic coupling matrix element for reactants a and b, and ΔG is the free energy of the electron-transfer reaction. The weighted sum is termed an effective Franck−Condon density of states for the acceptor ground state with the vibrationally excited state of the product and is taken over quantized vibrational states of the product with energies $n_f h\nu$. The S terms are Huang−Rhys electron-vibration coupling constants for each vibrational mode where $S = \Delta^2/2h$ and Δ is the dimensionless mode displacement. $W(R, T)$ is dependent on the reaction distance R through the coupling matrix element, which behaves exponentially as

$$H_{ab}{}^2 = \alpha \exp(-\beta[R - R_0]) \tag{7}$$

Here, α is the coupling matrix element for a donor−acceptor pair at van der Waals separation R_0 and β is a constant scaling the distance dependence. The distance dependence of the rate is also manifested through the reorganization energy. Assuming spherical initial (i) and final (f) states, the solvent reorganization energy can be expressed as[44]

$$\lambda = \left(\frac{1}{\epsilon_{opt}} - \frac{1}{\epsilon_s}\right)\left(\frac{1}{2r_i} + \frac{1}{2r_f} - \frac{1}{R}\right) \tag{8}$$

where ϵ_{opt} and ϵ_s are the optical and static dielectric constants of the solvent, respectively.

The basics of Marcus theory demonstrate that an electron-transfer rate will be maximized when the barrier for the process is minimized. The rate maximizes when $\Delta G + \lambda + n_f h\nu = 0$ and, under this condition, is governed solely by the Franck−Condon factors and coupling matrix element (at a distance R). For most systems displaying large changes in free energy, a combination of multiple internal vibrational modes and solvent modes can almost always provide the required energy matching and maximize the rate.

The reaction free energy of nitrobenzene with $(e^-)_{aq}$ at room temperature is known to be $\Delta G = -2.38$ eV.[33,45] Calculated values of ΔG_f are available for $(e^-)_{aq}$ from 0 to 250 °C.[46] If we assume that ΔG_f for nitrobenzene is constant up to 300 °C, we can estimate the change in free energy for reaction 1 with temperature. The temperature-dependent ΔG is shown in Figure 5. Also illustrated in Figure 5 is the temperature dependence of λ (eq 8) at infinite R, taking into account changes in dielectric constant and $(e^-)_{aq}$ radius with temperature. If we assume that the electron-transfer rate for reaction 1 is maximized and, hence, $-\Delta G \cong \lambda$, then we can solve for values of R that give $\lambda - \Delta G = 0$ at each temperature. The result is shown in Figure 6. This plot illustrates that allowing $-\Delta G \cong \lambda$ at all temperatures requires unphysically large values for R. To obtain sensible R values, the solvent reorganization energy must be lower, dictating that reaction 1 must occur in the Marcus inverted region ($\lambda < \Delta G$) at all temperatures.

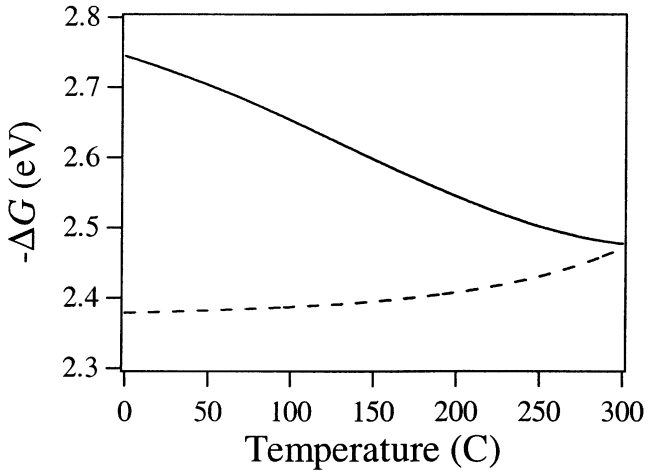

Figure 5. Temperature dependence of the free energy change (dashed line) and solvent reorganization energy at infinite reaction distance (solid line) for reaction 1.

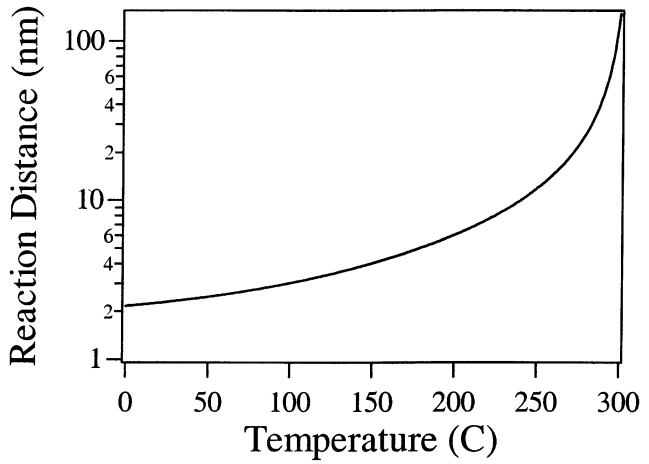

Figure 6. Optimum reaction distance for reaction 1 calculated via eqs 8 and 9, based on setting $-\Delta G = \lambda$ to achieve a barrierless electron transfer.

By convention, to say that a reaction is diffusion-limited implies that it occurs with unit probability upon contact of the reactants. For a long-range electron-transfer reaction, contact need not occur. Nonetheless, diffusion still takes a role in determining the rate. The combined diffusion and distance-dependent reaction can be solved in the framework of the Smoluchowski equation by invoking the radiation boundary condition.[47,48] An exponential distance dependence is assumed for the electron-transfer probability, $p(r) = \alpha \exp(-\beta r)$ (i.e., the behavior of H_{ab}^2), and R is replaced by

$$R^* = \frac{2}{\beta}\left[0.577 + \ln\left[\frac{1}{\beta}\left(\frac{\alpha}{D}\right)^{1/2}\right] + \frac{K_0(x) - yK_1(x)}{I_0(x) - yI_1(x)}\right] \quad (9)$$

with

$$x = \frac{2}{\beta}\left(\frac{\alpha}{D}\right)^{1/2} \exp\left(-\frac{a\beta}{2}\right) \quad \text{and} \quad y = \frac{ax\beta}{2}$$

Here a is the diffusional "distance of closest approach", and $I_{0,1}$ and $K_{0,1}$ are modified Bessel functions of the first and second kind, respectively. This equation had been previously applied to rate constant data obtained below 100 °C,[33] where the parameters α and β were iterated to give the best overall fit to the reaction distance. Typical values for long-range electron-transfer reactions were obtained with $\alpha = 2.5 \times 10^{13}$ s^{-1} and $\beta = 0.75$ Å^{-1}. The raw data and fitted curve corresponding to these values are shown in Figure 4, indicated by the squares and solid line, respectively. The triangles correspond to the new data taken up to 300 °C, and the dashed line illustrates the best possible fit to both data sets, given by the values $\alpha = 1.6 \times 10^{13}$ s^{-1} and $\beta = 0.90$ Å^{-1}. A more reasonable fit could be obtained by introducing a temperature-dependent β that decreases with increasing temperature. The $(e^-)_{aq}$ diffusion coefficient values are unknown above 150 °C, and our extrapolation to higher temperatures is also a possible source of error. The data require either a decrease in β or an increase of the already very high $(e^-)_{aq}$ diffusional activation energy between 150° and 300 °C.

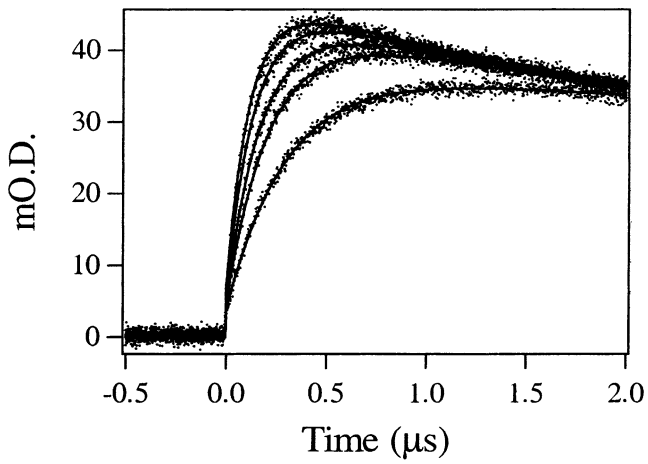

Figure 7. Sample fitted data for OH• radical scavenging by nitrobenzene at 225 °C and 250 bar. Nitrobenzene concentrations range from 5.73×10^{-4} to 2.82×10^{-3} M, corresponding to the longest through shortest observed rise rates.

B. Hydroxyl Radical Scavenging. In this section, we first give an overview of the experimental kinetic and transient spectral results of OH• radical reactivity with nitrobenzene. A kinetic model is then presented and used to assign the observed spectral features and fit the kinetics. We then compare these results to those of ref 12, pointing out both similarities and discrepancies.

1. Overview of Data. Directly monitoring changes in OH• concentration as it reacts with nitrobenzene (reaction 2) is difficult because of its deep ultraviolet absorption and low extinction coefficient ($\epsilon_{225\ nm} = 500$ M^{-1} cm^{-1}).[10] The nitrohydroxycyclohexadienyl radical has an absorption maximum at 400 nm and a moderate extinction coefficient of 5660 M^{-1} cm^{-1}.[13] Therefore, we monitored the concentration increase of the reaction product rather than the concentration decrease of the OH• radical. The OH• radical can add to nitrobenzene in three different positions to form three isomers. Data showing the differences in absorption spectra for these isomers are unavailable to our knowledge and their spectra are assumed to coincide. The reaction follows pseudo-first-order kinetics in the presence of excess nitrobenzene. Nitrobenzene concentrations used ranged from 2×10^{-4} to 6×10^{-3} M, and initial OH• concentrations upon radiolysis were $\sim 5 \times 10^{-6}$ M, giving conditions well within the pseudo-first-order limit.

A study of hydroxyl radical scavenging by nitrobenzene (reaction 2) was carried out as a function of temperature up to 400 °C. All data were collected at a pressure of 250 bar except at 380 and 400 °C, where the pressure was 300 bar. Sample fitted kinetic data taken at 225 °C are shown in Figure 7. The growth in the data represents the formation of the nitrohydroxy-

cyclohexadienyl radical product transient absorption at 400 nm. Nitrobenzene concentrations range from 5.73×10^{-4} to 2.82×10^{-3} M, corresponding to the longest through shortest observed rise rates. Although the rise rate would follow pseudo-first-order kinetics in the absence of interfering reactions, we chose to fit the data with a system of differential equations (described below).

Time-resolved transient absorption spectra were obtained in the wavelength range of 320−520 nm nearly every 25 °C from 150° up to 400 °C. Two examples are shown in Figure 8 (note the longer time scale compared to Figure 7) where the top panel (8a) shows data collected at 225 °C and the bottom panel (8b) shows data at 350 °C. At 225 °C, the initial product absorption is observable with an absorption maximum at 415 nm. The absorption shows a slight blue shift with temperature, shifting to 405 nm at 350 °C and 400 nm at 400 °C. As discussed below, the absorption decays via second-order kinetics up to 225 °C and at higher temperatures decays with a small first-order component as well. The transient spectra indicate a residual absorption remains at longer times that is immediately observable after the linac pulse at all wavelengths and temperatures. A maximum for this absorption is not observed within the wavelength range studied; however, its intensity increases toward shorter wavelengths. Under all conditions, the residual absorption does not decay on the experimental time scale. Its relative intensity becomes greater with increasing temperature. The transient spectra also indicate the growth of another feature in the 330 nm region with an ∼40 μs time constant. The intensity of this feature increases toward shorter wavelengths, and the absorption maximum is not observed within the measured wavelength region. The growth rate does not appear to be temperature-dependent, but the absorption either intensifies or red shifts with increasing temperature. The signal-to-noise ratio in this wavelength region is insufficient to determine whether this feature decays by first or second-order kinetics.

2. Kinetic Model and Spectral Assignments. Based on the features observed in the transient spectra and other data existing in the literature,[13] a model to fit the observed kinetics at 400 nm is described by the reaction set:

$$C_6H_5NO_2 + (e^-)_{aq} \rightarrow C_6H_5NO_2^{\bullet -} \quad (1)$$

$$C_6H_5NO_2 + OH^\bullet \rightarrow C_6H_5NO_2(OH^\bullet) \quad (2)$$

$$C_6H_5NO_2 + H^\bullet \rightarrow C_6H_5NO_2(H^\bullet) \quad (10)$$

$$2C_6H_5NO_2(OH^\bullet) \rightarrow \text{products} \quad (11)$$

$$C_6H_5NO_2(OH^\bullet) \rightarrow \text{products} \quad (12)$$

$$2C_6H_5NO_2(H^\bullet) \rightarrow \text{products} \quad (13)$$

$$C_6H_5NO_2(H^\bullet) \rightarrow \text{products} \quad (14)$$

$$OH^\bullet + OH^\bullet \rightarrow H_2O_2 \quad (15)$$

The observed absorption near 415 nm is assigned to the product of reaction 2 and, at higher temperatures, reactions 2 and 10. $C_6H_5NO_2(OH^\bullet)$ has been previously reported to absorb at this wavelength, and the wavelength shift with temperature roughly correlates with prior data.[12] No temperature-dependent spectral data are available for $C_6H_5NO_2(H^\bullet)$. However, it has been known for decades that aromatic molecules including nitrobenzene

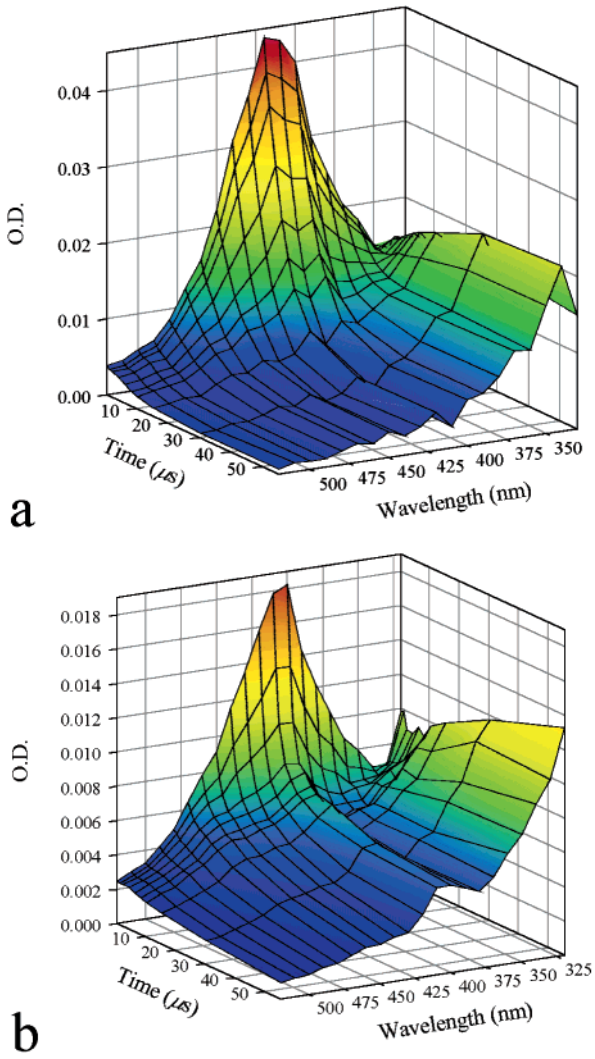

Figure 8. Time-resolved transient absorption spectra in the region of the $C_6H_5NO_2(OH^\bullet)$ product absorption at (a) 225 and (b) 350 °C and 250 bar.

display similar absorptions for both the $OH^\bullet$ and $H^\bullet$ radical complexes at room temperature.[49−52] Furthermore, the room-temperature addition rate constants are similar for nitrobenzene.[53] On the basis of existing fast electron radiolysis yield measurements,[7,54] $H^\bullet$ atoms should account for ∼20% of the total radiolysis products at 300 °C. The percentage is smaller at lower temperatures and has a value of ∼10% at 200 °C. With this percentage of $H^\bullet$ atoms available to react, the total nitrobenzene complex product absorption should be <20% $C_6H_5NO_2(H^\bullet)$ at all temperatures below 300 °C. However, the N_2O present in these experiments rapidly converts $(e^-)_{aq}$ to $OH^\bullet$ radicals (reactions 3 and 4), nearly doubling the $OH^\bullet$ yield. This decreases the amount of possible absorption by $C_6H_5NO_2(H^\bullet)$ to <15% (much less at lower temperatures). At 300 °C and above, O_2 was added to the nitrobenzene solution to act as an $H^\bullet$ atom scavenger for two reasons: (1) the relative radiolysis yield of $H^\bullet$ atoms increases substantially at higher temperatures[7] and (2) preliminary studies of the reaction of $OH^\bullet$ with H_2 gas using reaction 2 as a competition partner demonstrate $H^\bullet$ atom reactivity with nitrobenzene above 300 °C.[55] Rate constant data for $H^\bullet$ atom scavenging by O_2 is available up to 225 °C.[25] On the basis of an extrapolation of these data and our concentration of O_2, we estimate that $H^\bullet$ atom scavenging should occur with a ≤7 ns time constant in the ≥300° C region, ensuring that we only observe the $C_6H_5NO_2(OH^\bullet)$ product. The loss of C_6H_5-

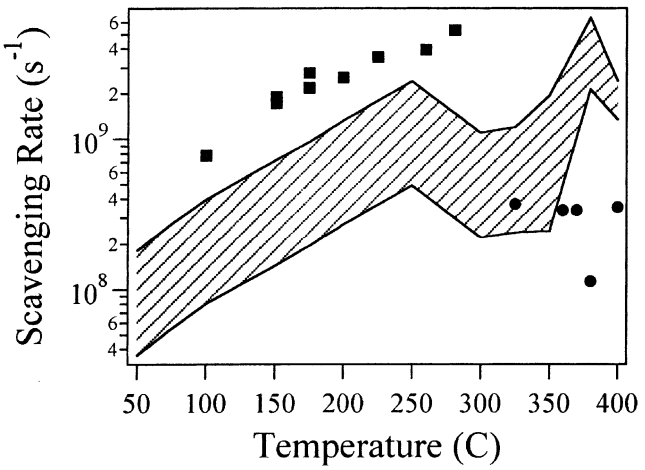

Figure 9. Predicted hydrated electron scavenging rates for N_2O (squares), O_2 (circles), and nitrobenzene (patterned area). The patterned area corresponds to the range of nitrobenzene concentrations used at each temperature. N_2O and O_2 molal concentrations were constant for all experiments.

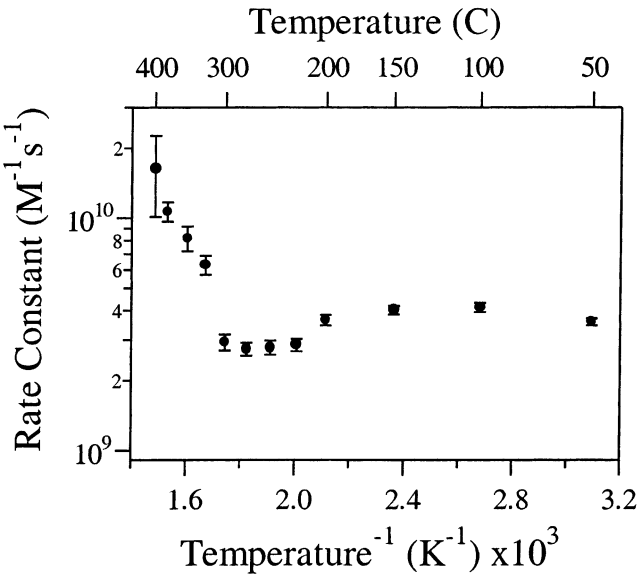

Figure 10. Arrhenius plot for the reaction of nitrobenzene with OH• radicals.

TABLE 3: Fitted Rate Constants for Hydroxyl Radical Scavenging by Nitrobenzene (reaction 2)

temp (C)	rate constant ($M^{-1}s^{-1}$) × 10^{-9}	temp (C)	rate constant ($M^{-1}s^{-1}$) × 10^{-9}
50	3.6 ± 0.1	275	2.7 ± 0.2
100	4.1 ± 0.2	300	2.9 ± 0.2
150	4.0 ± 0.2	325	6.3 ± 0.6
200	3.6 ± 0.2	350	8.2 ± 1.0
225	2.9 ± 0.2	380	10.7 ± 1.0
250	2.8 ± 0.2	400	16.4 ± 6.2

$NO_2(OH^•)$ and $C_6H_5NO_2(H^•)$ is described by a combination of reactions 11−14, accounting for the observed combined first and second-order decay kinetics. Reactions 11 and 13 are expected to dominate the product decay at lower temperatures, where the data show mostly second-order behavior.

The observed residual absorption is assigned to the nitrobenzene radical anion formed in reaction 1. The nitrobenzene anion has been studied at room temperature via spectroelectrochemistry.[56] It displays an intense, narrow UV absorption band at 325 nm but has other overlapping bands throughout the visible spectrum with weaker intensity. On the basis of the measured rate constants for reaction 1 (see Figure 2), nitrobenzene will compete with O_2 and N_2O to scavenge $(e^-)_{aq}$ and eventually become the dominant scavenger at the highest temperatures recorded. Figure 9 shows the expected range of rates for $(e^-)_{aq}$ scavenging (reaction 1) based on the upper and lower nitrobenzene concentrations used during the OH• addition experiments. Also displayed are the expected $(e^-)_{aq}$ scavenging rates[7,57] for O_2 and N_2O in the temperature ranges where they were each used in these experiments. By taking the ratio of the N_2O scavenging rates to the maximum nitrobenzene rates, it can be determined that nitrobenzene will scavenge <40% of the $(e^-)_{aq}$ in the presence of N_2O at all temperatures. Up to ∼95% of the $(e^-)_{aq}$ will be scavenged by nitrobenzene in the presence of O_2 at and above the critical temperature, and up to ∼85% may be scavenged at sub-critical temperatures. This correlates well with our experimental observations, where the residual absorption notably increases as the temperature is raised and the switch is made at 300 °C from using N_2O to less soluble O_2. The nitrobenzene radical anion is very long-lived (100's of μs) at all temperatures.

Reaction 15 is included in the modeling to account for possible loss of OH• by a competing bimolecular recombination reaction. The rate constant for reaction 15 is extrapolated from available data below 215 °C.[25] Inclusion of this low activation energy reaction in the modeling affects the fitted rates by <5% and becomes less important with increasing temperature.

The growth of the feature in the 330 nm region with a ∼40 μs time constant could be due to the eventual formation of dinitrodihyroxybiphenyl and dinitrobiphenyl product species formed through reactions 11 and 13, where the reactions proceed as a dimerization of the radical species. We were unable to find spectral data for dinitrodihyroxybiphenyl, but the absorption for dinitrobiphenyl has been shown to occur in the 300 nm region.[58] On the basis of Woodward's rules for substituted organics, it is likely that dinitrodihyroxybiphenyl would be red-shifted ∼30 nm compared to dinitrobiphenyl because of the presence of two hydroxyl groups. However, the observed ∼40 μs rise time for the growth of this feature does not correlate with the <10 μs decay of the radical species absorption unless an additional intermediate species is involved which is not observed in this wavelength region. Because the UV absorption for this feature is significantly removed from the kinetics monitored at 400 nm, its presence is ignored in the data fitting.

Several simplifications were made to the reaction scheme for fitting the growth kinetics, i.e., the rate of reaction 2. The experimental data were truncated at 2−4 μs after the linac pulse, and the decay of the product absorption was fit using first-order kinetics. Although the decay of the product absorption follows some combination of first and second-order kinetics, simulations show that the second-order kinetics can be approximated by a first-order decay within the first half-life. In the presence of N_2O, the radiolysis yield of H• atoms below 300 °C is <15% of the total species formed. This yield increases above 300 °C, but in this range, we have added in O_2 as an H• atom scavenger. Therefore, the $C_6H_5NO_2(H^•)$ complex is thought to account for <15% of the total product yield under all conditions, and its reactions are neglected. Hence, the fit incorporates pseudo-first-order growth of the $C_6H_5NO_2(OH^•)$ species and first-order decay, along with possible bimolecular recombination of the OH• radicals. The presence of the nitrobenzene radical anion is modeled via a baseline offset immediately after the linac pulse.

An Arrhenius plot of the extracted growth rate constants is shown in Figure 10 and the rate constants are given in Table 3. The data points shown represent an average of the fitted rate

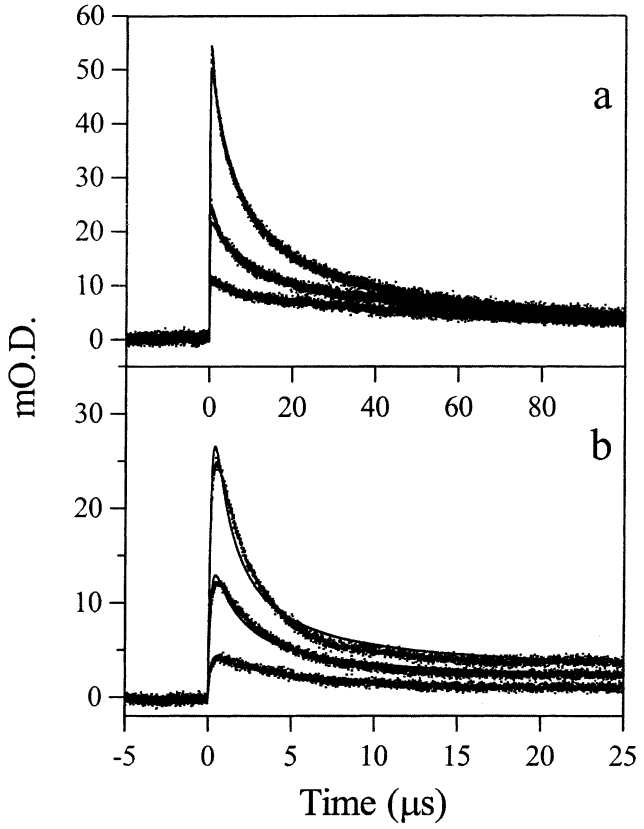

Figure 11. Sample data showing the $C_6H_5NO_2(OH^•)$ product growth and decay at (a) 150 °C and (b) 300 °C and 250 bar at 400 nm. Note the two different time scales for a and b. The decays at 150 °C follow nearly second-order kinetics and at 300 °C show a mixture of first and second-order behavior. The residual absorption in b at long times is due to the nitrobenzene radical anion, which does not decay on the experimental time scale.

constants obtained for the five nitrobenzene concentrations run at each temperature. The error bars shown represent one standard deviation of this average. As previously reported,[11,12] the rate constant is insensitive to temperature up to 300 °C. It then increases gradually as the critical temperature is approached and surpassed. In ref 12, this increase was not observed until the critical temperature was reached. Reference 12 reported only a factor of ~2 increase relative to the rate below 300 °C, whereas our results show a factor of ~6. In addition, ref 12 showed a clear dip in the rate constant at 275 °C which we do not observe. Possible reasons for these discrepancies are discussed below.

It was not our purpose to extensively study the decay of the product species, so long time scale data are not available at all of the temperatures listed in Table 3. However, with the product growth rates in hand, the available long time scale data were also fit to discern the decay rate of the product absorption. Second-order kinetics dominate the product absorption decay at all temperatures, but the presence of a small first-order decay also becomes apparent above 225 °C. Fitting the entire decay to concurrent first and second-order decays does not give good results for the first-order decay rate constant because of fluctuations in the baseline at longer times, and we merely approximated the decay with the dominant second-order kinetics and residual absorption. Figure 11a shows kinetic data at 400 nm collected at 150 °C. The three traces represent three applied radiation doses, where the largest dose corresponds to the highest change in O.D. As expected for a second-order decay, the absorption lifetime decreases as the initial amount of signal increases, and all three traces coincide at long times. The product

TABLE 4: Fitted Second-Order Rate Constants for the Decay of the $C_6H_5NO_2(OH^•)/C_6H_5NO_2(H^•)$ Product Absorption[a]

temp (C)	rate constant ($M^{-1}s^{-1}$)	temp (C)	rate constant ($M^{-1}s^{-1}$)
50	$7.0 \pm 1.0 \times 10^9$	300	$2.8 \pm 0.7 \times 10^{11}$
100	$2.1 \pm 0.4 \times 10^{10}$	325	$1.1 \pm 0.3 \times 10^{12}$
150	$1.9 \pm 0.4 \times 10^{10}$	350	$1.9 \pm 0.5 \times 10^{12}$
225	$6.8 \pm 2.1 \times 10^{10}$		

[a] Note: values above 225 °C are suspect due to presence of an additional first-order decay.

absorption lifetime decreases substantially as the temperature is raised. The half-life decreases from ~7 μs at 150 °C to ~3 μs at 300 °C at the highest measured doses. Figure 11b illustrates the kinetics at 300 °C and clearly displays the greater baseline offset at higher temperatures because of higher concentrations of the nitrobenzene radical anion. The need for a first-order component becomes apparent in Figure 11b, as the fit to the decay is poor compared to Figure 11a. The second-order rate constants were fitted as $2k/\epsilon$, and fitted second-order rate constants (k) are given in Table 4. The extinction coefficient ϵ was taken as 5560 M^{-1} cm^{-1} and was assumed to be independent of temperature.[13] An Arrhenius fit to the data up to 225 °C gives 15.8 ± 0.2 kJ/mol, very close to the 15.0 kJ/mol activation energy for self-diffusion in water, as predicted by the slope of $T/\eta(T)$ for water from room temperature up to 225 °C. An Arrhenius fit from 225° to 350 °C gives a ridiculously high activation energy of 68 ± 13 kJ/mol, again indicating the need for a first-order component in this region and possibly a decrease in the extinction coefficient of the product absorption. Where the second-order decay probably represents a dimerization of the initial products to form dihydroxydinitrobiphenyl and dinitrobiphenyl compounds, the first-order decay may indicate some decomposition of the initial products.

3. Comparison to Prior Results. Two aspects of the experiments reported in ref 12 may explain the disagreement with our data at higher temperatures. First, the data of ref 12 were fit using a simple single-exponential growth to a plateau where we used a more complete differential equation model incorporating the multiple kinetic features at hand. Second and more importantly, H• atoms formed via radiolysis were not scavenged in ref 12.

Approximating the growth kinetics by fitting a simple single-exponential rise to a plateau is most accurate in the limit where the product decay is very slow compared to the growth. As evidenced by data shown here, the decay of the product absorption becomes faster at higher temperatures. At 50 °C, the decay half-life is ~50 μs, whereas in the supercritical region, it is ~500 ns. The faster product decay at higher temperatures will affect the apparent growth rate if the decay is not incorporated into the data fitting. Consequently, the need for incorporating the decay time becomes more crucial as the decay times approach the rise times, i.e., at higher temperatures. Fitting sample data at 380 °C with just a single-exponential growth shows a ~30% difference in the extracted rate constant when compared with fits using the differential equation model. The error becomes smaller with decreasing temperature and by 275 °C shows only a ~15% difference. At 50 °C, the same results are obtained with both fitting models.

It has been previously demonstrated that the radiolysis yield of H• atoms relative to $(e^-)_{aq}$ becomes greater with decreasing water density and increasing temperature.[7] Below 300 °C, the ratio of H• atoms to $(e^-)_{aq}$ is <0.5, but by 350 °C, it is ~1.1.

The radiolysis yield increase of $OH^{\bullet}$ radicals from 300° to 350 °C is only ~5%.[59] This implies a greater overall contribution of $H^{\bullet}$ atoms to the radiolysis yield at higher temperatures. With relatively more $H^{\bullet}$ atoms available, the relative yield of the $C_6H_5NO_2(H^{\bullet})$ product versus $C_6H_5NO_2(OH^{\bullet})$ should increase. Therefore, the product growth observed at 400 nm will no longer be solely due to $C_6H_5NO_2(OH^{\bullet})$ if no $H^{\bullet}$ atom scavenger is present. The observed growth should follow pseudo-first-order kinetics, but should be biexponential because two species are being formed. If the rate constants for formation of $C_6H_5NO_2(H^{\bullet})$ and $C_6H_5NO_2(OH^{\bullet})$ are similar within a factor of ~3, separation of the two growth terms will be impossible with typical signal-to-noise levels, and the growth will appear as a single exponential. The rate constant for formation of $C_6H_5NO_2(H^{\bullet})$ at room temperature[53] is 2.3×10^9 compared to 2.5×10^9 for $C_6H_5NO_2(OH^{\bullet})$. Because the rate constants are so similar, separation of the two species at room temperature is impossible without use of a scavenger. If the rate constant for formation of $C_6H_5NO_2(H^{\bullet})$ decreases at elevated temperatures relative to that for $C_6H_5NO_2(OH^{\bullet})$, this could explain the discrepancy between the rate constants reported here and in ref 12. Dramatically decreasing rate constants for addition of the muonium atom (an unstable light isotope of hydrogen) to benzene in this temperature range has in fact been observed by Ghandi et al.[60]

To explain the behavior of the reaction 2 rate constant up to 200 °C, Ashton et al.[11] proposed a model that breaks down reaction 2 into three steps

$$C_6H_5NO_2 + OH^{\bullet} \rightarrow [C_6H_5NO_2(OH^{\bullet})]_{\pi} \qquad (16)$$

$$[C_6H_5NO_2(OH^{\bullet})]_{\pi} \rightarrow C_6H_5NO_2 + OH^{\bullet} \qquad (17)$$

The $OH^{\bullet}$ addition in reaction 16 is presumed to form a π-bonded

$$[C_6H_5NO_2(OH^{\bullet})]_{\pi} \rightarrow [C_6H_5NO_2(OH^{\bullet})]_{\sigma} \qquad (18)$$

intermediate that can dissociate to give back the reactants (reaction 17) or proceed to form the observed σ-bonded intermediate (reaction 18). Reaction 16 is assumed to be diffusion-limited, whereas reactions 17 and 18 have activation barriers. The reaction 16 rate constant was calculated via the Smoluchowski equation (eq 5), and the activation energies and preexponential factors were fit to experimental data by Ashton et al. Feng et al. extended this model to 390 °C, making improvements to the reactant radii and diffusion coefficients.[12] The experimental data up to 225° C were used to define the "apparent" Arrhenius parameters. Feng et al. found the improved three-step mechanism satisfactory in explaining their experimental result using the same "apparent" Arrhenius parameters up to 390 °C. However, the model underestimates our measured rate constants above 300 °C. We do not discount the proposed reaction set, but it is probable that the activation energies deduced from data below 225 °C have different values at higher temperatures. Numerous other reactions have demonstrated temperature-dependent activation energies, especially in the critical region.[4,7,57,60]

IV. Conclusions

The rate constants for the reactions of nitrobenzene with the hydroxyl radical and hydrated electron in water have been measured from room temperature to 400 °C using pulse radiolysis and transient absorption spectroscopy. The activation energy for the diffusion-limited reaction of nitrobenzene with $(e^-)_{aq}$ is relatively insensitive to temperature up to 300 °C, indicating that the activation energy for electron diffusion remains relatively high over this entire range. The estimated reaction radii at each temperature suggest a long-range electron-transfer mechanism. The energetics of the reaction guarantee Marcus inverted region behavior. Above 300 °C, the rate constant continues to increase, but the reaction has a smaller activation energy. Just above the critical temperature, the rate constant displays a density dependence similar to that previously reported for other $(e^-)_{aq}$ scavenging reactions involving hydrophobic species.

The rate constant for the reaction of nitrobenzene with $OH^{\bullet}$ is insensitive to temperature from room temperature to 300 °C, confirming previous results.[11,12] The product nitrohydroxycyclohexadienyl radical absorption near 400 nm decays by second-order kinetics, and the reaction has approximately diffusion-limited activation energy. Above 300 °C, the rate constant for $OH^{\bullet}$ addition to nitrobenzene increases as the critical point is approached and exceeded. Time-resolved electronic absorption spectra of the nitrobenzene radiolysis products reveal multiple absorbing species exhibiting complex kinetics. The second-order decay of the product at 400 nm becomes complicated by a first-order component, and the absorption of the UV-absorbing product becomes stronger. Hydrogen atom addition to the nitrobenzene becomes much more important above 300 °C, necessitating the use of O_2 as a scavenger for $H^{\bullet}$ atoms to isolate the $OH^{\bullet}$ addition reaction. The signals become smaller, and the very high reaction rate of nitrobenzene with $(e^-)_{aq}$ dictates that the nitrobenzene radical anion absorption cannot be ignored. For all of these reasons, we recommend nitrobenzene as a competition partner for $OH^{\bullet}$ radical kinetic studies only up to ~300 °C.

Acknowledgment. We thank Dr. Sergey Chemerisov for operating the linac accelerator used in this work. T.W.M., J.A.C., and K.T. were supported under NERI Grant No. M9SF99-0276. We also thank the Ministry of Education in Japan for additional financial support to K. Takahashi. The submitted manuscript has been created by the University of Chicago as Operator of Argonne National Laboratory ("Argonne") under Contract No. W-31-109-ENG-38 with the U.S. Department of Energy. The U.S. Government retains for itself, and others acting on its behalf, a paid-up, nonexclusive, irrevocable worldwide license in said article to reproduce, prepare derivative works, distribute copies to the public, and perform publicly and display publicly, by or on behalf of the Government.

References and Notes

(1) Oka, Y.; Koshizuka, C. *Prog. Nucl. Energy* **1998**, *32*, 163.

(2) Bushby, S. J.; Dimmick, G. R.; Duffey, R. B.; Burrill, K. A.; Chan, P. S. W. *Conceptual designs for advanced, high-temperature CANDU reactors*; ICONE 8: 8th International Conference on Nuclear Engineering, Baltimore, MD, 2000.

(3) SCR2000. *Proceedings of The First International Symposium on Supercritical Water-Cooled Reactors, Design and Technology*; The First International Symposium on Supercritical Water-Cooled Reactors, Design and Technology, Tokyo, Japan, 2000.

(4) Elliot, A. J. *Rate Constants and G-Values for the Simulation of the Radiolysis of Light Water over the Range 0−300°C*; report AECL-11073, Atomic Energy of Canada, Ltd., 1994.

(5) EPRI. *Proceedings: 1989 Workshop on LWR Radiation Water Chemistry and Its Influence on In−Core Structural Materials*; Workshop on LWR Radiation Water Chemistry and Its Influence on In−Core Structural Materials, 1989.

(6) Cohen, P. *Water Coolant Technology of Power Reactors*; Gordon and Breach: New York, 1969.

(7) Cline, J. A.; Takahashi, K.; Marin, T. W.; Jonah, C. D.; Bartels, D. M. *J. Phys. Chem. A* **2002**, *106*, 12260.

(8) Asmus, K.-D.; Cercek, B.; Ebert, M.; Henglein, A.; Wigger, A. *Trans. Faraday Soc.* **1967**, *63*, 2435.
(9) Neta, P.; Dorfman, L. M. *Adv. Chem. Ser.* **1968**, *81*, 222.
(10) Buxton, G. V.; Greenstock, C. L.; Helman, W. P.; Ross, A. B. *J. Phys. Chem. Ref. Data* **1988**, *17*, 513.
(11) Ashton, L.; Buxton, G. V.; Stuart, C. R. *J. Chem. Soc., Faraday Trans.* **1995**, *91*, 1631.
(12) Feng, J.; Aki, S.; Chateauneuf, J. E.; Brennecke, J. F. *J. Am. Chem. Soc.* **2002**, *124*, 6304.
(13) Pozdnyakov, I. P.; Glebov, E. M.; Plyusnin, V. F.; Grivin, V. P.; Ivanov, Y. V.; Vorobyev, D. Y.; Bazhin, N. M. *Pure Appl. Chem.* **2000**, *72*, 2187.
(14) Barat, F.; Gilles, L.; Hickel, B.; Lesigne, B. *J. Phys. Chem.* **1973**, *77*, 1711.
(15) Hankiewicz, E.; Schulte-Frohlinde, D. *J. Phys. Chem.* **1977**, *81*, 2614.
(16) Milosavljevic, B. H.; Micic, O. I. *J. Phys. Chem.* **1978**, *82*, 1359.
(17) Afanassiev, A. M.; Okazaki, K.; Freeman, G. R. *Can. J. Chem.* **1979**, *57*, 839.
(18) Afanassiev, A. M.; Okazaki, K.; Freeman, G. R. *J. Phys. Chem.* **1979**, *83*, 1244.
(19) Idriss-Ali, K. M.; Freeman, G. R. *Can. J. Chem.* **1984**, *62*, 2217.
(20) Cygler, J.; Freeman, G. R. *Can. J. Chem.* **1984**, *62*, 1265.
(21) Maham, Y.; Freeman, G. R. *J. Phys. Chem.* **1985**, *89*, 4347.
(22) Maham, Y.; Freeman, G. R. *Can. J. Chem.* **1988**, *66*, 1706.
(23) Sedigallage, A. P.; Freeman, G. R. *Can. J. Phys.* **1990**, *68*, 940.
(24) Cercek, B. *Nature* **1969**, *223*, 491.
(25) Elliot, A. J.; McCracken, D. R.; Buxton, G. V.; Wood, N. D. *J. Chem. Soc., Faraday Trans.* **1990**, *86*, 1539.
(26) Lai, C. C.; Freeman, G. R. *J. Phys. Chem.* **1990**, *94*, 302.
(27) Peiris, S. A.; Freeman, G. R. *Can. J. Chem.* **1991**, *69*, 884.
(28) Takahashi, K.; Cline, J. A.; Bartels, D. M.; Jonah, C. D. *Rev. Sci. Instrum.* **2000**, *71*, 3345.
(29) Bartels, D. M.; Takahashi, K.; Cline, J. A.; Marin, T. W.; Jonah, C. D. To be published.
(30) Cline, J. A.; Jonah, C. D.; Bartels, D. M. *Rev. Sci. Instrum*. **2002**, *73*, 3908.
(31) Lee, D. S.; Park, S. D. *J. Haz. Mater.* **1996**, *51*, 67.
(32) Savage, P. E. *Chem. Rev.* **1999**, *99*, 603.
(33) Schmidt, K. H.; Han, P.; Bartels, D. M. *J. Phys. Chem.* **1995**, *99*, 10530.
(34) Christensen, H.; Sehested, K. *J. Phys. Chem.* **1986**, *90*, 186.
(35) *Diffusion-Limited Reactions*; Rice, S. A., Ed.; Elsevier: Amsterdam, 1985; Vol. 25, p 404.
(36) Hynes, J. T. *Theory of Chemical Reaction Dynamics*; CRC Press: Boca Raton, FL, 1985; Vol. IV.
(37) Han, P.; Bartels, D. M. *J. Phys. Chem.* **1996**, *100*, 5597.
(38) Weast, R. *CRC Handbook of Chemistry and Physics*, 52nd ed.; CRC Press: Boca Raton, FL, 1971.
(39) Jortner, J. *J. Chem. Phys.* **1976**, *64*, 4860.
(40) Closs, G. L.; Miller, J. R. *Science* **1988**, *240*, 440.
(41) Suppan, P. *Top. Curr. Chem.* **1992**, *163*, 95.
(42) Meyer, T. J. *Prog. Inorg. Chem.* **1983**, *30*, 389.
(43) Barbara, P. F.; Meyer, T. J.; Ratner, M. A. *J. Phys. Chem.* **1996**, *100*, 13148.
(44) Brunschwig, B. S.; Ehrenson, S.; Sutin, N. *J. Phys. Chem.* **1986**, *90*, 3657.
(45) Wardman, P. *J. Phys. Chem. Ref. Data* **1989**, *18*, 1637.
(46) Shiraishi, H.; Sunaryo, G. R.; Ishigure, K. *J. Phys. Chem.* **1994**, *98*, 5164.
(47) Kuznetsov, A. M.; Ulstrup, J. *Chem. Phys. Lett.* **1983**, *97*, 285.
(48) Sipp, B.; Voltz, R. *J. Chem. Phys.* **1983**, *79*, 434.
(49) Land, E. J.; Ebert, M. *Trans. Faraday Soc.* **1967**, *63*, 1181.
(50) Wander, R.; Neta, P.; Dorfman, L. M. *J. Phys. Chem.* **1968**, *72*, 2946.
(51) Dorfman, L. M.; Taub, I. A.; Buhler, R. E. *J. Chem. Phys.* **1962**, *36*, 3051.
(52) Chutny, B. *Nature* **1967**, *213*, 593.
(53) Neta, P.; Dorfman, L. M. *J. Phys. Chem.* **1969**, *73*, 413.
(54) Elliot, A. J.; Chenier, M. P.; Ouellette, D. C. *J. Chem. Soc., Faraday Trans.* **1993**, *89*, 1193.
(55) Marin, T. W.; Cline, J. A.; Bartels, D. M.; Jonah, C. D. To be published.
(56) Compton, R. G.; Dryfe, R. A. W.; Fisher, A. C. *J. Chem. Soc., Perkin Trans. 2* **1994**, *7*, 1581.
(57) Takahashi, K.; Ohgami, S.; Sawamura, S.; Marin, T. W.; Bartels, D. M.; Jonah, C. D. To be published.
(58) Zhezlov, A. B.; Zelentsov, S. V.; Oleinik, A. V. *High Energy Chem.* **1999**, *33*, 87.
(59) Katsumura, Y.; Wu, G.; Lin, M.; Muroya, Y.; Morioka, T.; Terada, Y.; Li, X. *Res. Chem. Intermed.* **2001**, *27*, 755.
(60) Ghandi, K.; Addison-Jones, B.; Brodovitch, J. C.; Kecman, S.; McKenzie, I.; Percival, P. W. *Physica B* In press.